

# High-Entropy Polar Regions Around the First Protostars

Matthew J. Turk<sup>1</sup>, Michael L. Norman<sup>1</sup>, Tom Abel<sup>2</sup>

## ABSTRACT

We report on simulations of the formation of the first stars in the Universe, where we identify regions of hot atomic gas ( $f_{\text{H}_2} < 10^{-6}$ ) at densities above  $10^{-14} \text{ g cm}^{-3}$ , heated to temperatures ranging between 3000 and 8000 K. Within this temperature range atomic hydrogen is unable to cool effectively. We describe the kinetic and thermal characteristics of these regions and investigate their origin. We find that these regions, while small in total mass fraction of the cloud, may be dynamically important over the accretion timescale for the central clump in the cloud, particularly as a chemical, rather than radiative, mechanism for clearing the polar regions of the accretion disk of material and terminating accretion along these directions. These inherently three-dimensional effects stress the need for multi-dimensional calculations of protostellar accretion for reliable predictions of the masses of the very first stars.

*Subject headings:* galaxies: formation; stars: formation; ISM: H II regions; cosmology: theory

## 1. Introduction

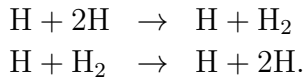
As the physical model that governs simulations of metal-free stars expands to include more chemical and radiative processes, the collapsing regions in which they are expected to form have revealed a variety of interesting phenomena (Yoshida et al. 2006; Turk et al. 2008; Clark et al. 2010; Turk et al. 2009; Stacy et al. 2010). The character of the inner regions of metal-free halos are strongly governed by the reactions that govern the formation and dissociation of molecular hydrogen at high densities (Turk et al. 2010b, submitted). At densities below  $10^{-16} \text{ g cm}^{-3}$ , the formation of molecular hydrogen is governed by electron-catalyzed association of  $\text{H}^-$  and  $\text{H}$  (Abel et al. 1997; Glover & Abel 2008). However, at densities of

---

<sup>1</sup>Center for Astrophysics and Space Science, University of California, San Diego

<sup>2</sup>Kavli Institute for Particle Astrophysics and Cosmology, Stanford University, 2575 Sand Hill Road, Menlo Park, CA 94025

$10^{-16}$  g cm $^{-3}$  and above, the formation of molecular hydrogen is dominated by three-body reactions, primarily where the third body is atomic hydrogen:



The reaction rates for these two reactions have been shown not only to be uncertain to an order of magnitude or more (Glover 2008) but these uncertainties may have a substantial impact on the structure and mass-distributions of collapsing primordial clouds (Turk et al. 2010b). Every molecule formed through this reaction releases 4.48 eV in thermal energy into the gas, and because the rate of formation decreases with increasing temperature, the overall process of transforming the atomic hydrogen gas in into a fully-molecular state occurs over several decades in density (Ripamonti & Abel 2004; Omukai & Nishi 1998; Galli & Palla 1998; Palla et al. 1983; Glover 2008). In 1D, spherically symmetric calculations it is inevitable that all high-density gas undergoes this transition. However, in full 3D calculations, the mechanism of transformation is more complex, owing to variations in the density-temperature distribution and the velocity structure of the collapsing cloud.

We present results of high-resolution computer simulations of metal-free star forming regions. In these simulations we identify regions of high-density ( $> 10^{-15}$  g cm $^{-3}$ ) atomic gas whose presence may contribute to a chemical, rather than radiative, mechanism for slowing or terminating accretion along the poles of primordial accretion disks (McKee & Tan 2008).

## 2. Simulations

We report on a single simulation drawn from a suite of calculations, designed to sample a variety of formation environments. We centered the simulation volume on the location of the peak density of the first dark matter halo of mass  $10^6 M_\odot$  to form and generated three nested subgrid levels, for an initial effective resolution of  $1024^3$ . Our initial conditions are generated as in Abel et al. (2002); O’Shea & Norman (2007), with the notable exception that we have updated our cosmological parameters to WMAP 7 (Jarosik et al. 2010; Turk et al. 2010a). These simulations were conducted using the code Enzo (O’Shea et al. 2004; Bryan & Norman 1998; Bryan et al. 2001), using a 9-species primordial chemistry model implementing the TWOSTEP method described in Verwer (1994) and in the appendix to Turk et al. (2009). While we focus on the effects of three-body molecular hydrogen formation with atomic hydrogen acting as the third body, we also solve the set of rate equations where molecular hydrogen acts as the third body. At densities of approximately  $10^{-15} - 10^{-13}$  g cm $^{-3}$ , primordial gas becomes optically thick to the cooling of molecular hydrogen from ro-vibrational transitions. In our simulations, this is applied using the prescription given in Ripamonti & Abel (2004),

which agrees well with the detailed Sobolev approximation (Turk et al. 2010b; Sobolev 1960; Yoshida et al. 2006). The cooling radiation is reduced by:

$$L_{\text{lines,thick}}(T) = L_{\text{lines,thin}} \times \min(1, (n/n_0)^{-\beta}),$$

with  $n_0 = 8 \times 10^9 \text{ amu cm}^{-3}$  and  $\beta = -0.45$  (Ripamonti & Abel 2004).

We discuss a relatively slow-collapsing halo that we can examine with some depth, but this halo is not extraordinary, nor does it fragment (Turk et al. 2009; Stacy et al. 2010; Clark et al. 2010). Furthermore, the phenomena discussed in this paper are present in a suite of simulations, and their frequency will be discussed in the forthcoming Turk et al. (2010a). The final output of the calculation at  $z = 17.4$ , has peak density of  $2.0 \times 10^{-9} \text{ g cm}^{-3}$  at the 29th level of refinement. The entire simulation has  $3.3 \times 10^7$  computational elements, including  $2.3 \times 10^6$  with cell size less than 35 AU.

We also introduce an improved refinement criterion as compared to previous simulations. We require the numerical resolution to be one sixteenth of the local Jeans length. However, the calculation of the Jeans length is done assuming the gas is at  $T_{\text{min}} = 200 \text{ K}$  even when it has not cooled so low. As a consequence we have  $(T/200\text{K})^{9/2}$  more resolution elements in the material before it forms the cold phase. We refer to this as the cold Jeans refinement criterion, which for all the material above the minimum temperature is more stringent than the standard criterion. This modification ensures high resolution at high densities even before the material forms the cooling cores. In addition, we also refine on overdensity in both baryonic and dark matter content at a factor of 4.0 which ensures high resolution in the lower density material that forms first star hosting mini halos.

### 3. Results

As the gas collapses and is converted to molecular hydrogen, we see a spread in the temperature and the molecular hydrogen fraction as a function of density, as shown in the upper left and upper right panels of Figure 1. At densities between approximately  $10^{-15} \text{ g cm}^{-3}$  and  $10^{-10} \text{ g cm}^{-3}$  the mass is distributed over a broad range of temperatures, while the corresponding spread in molecular hydrogen fractions is an order of magnitude or more. This results in a broad variation of the rate coefficients governing the transition to molecular hydrogen. For higher temperature gas, the overall transition occurs more slowly, resulting in less efficient ro-vibrational cooling. In some regions of phase space, the onset of the transformation of the gas is delayed until the onset of optical thickness.

In the upper left panel of Figure 1 we plot the distribution of mass as a function of density and temperature. The clear trend is for the gas to follow standard tracks through

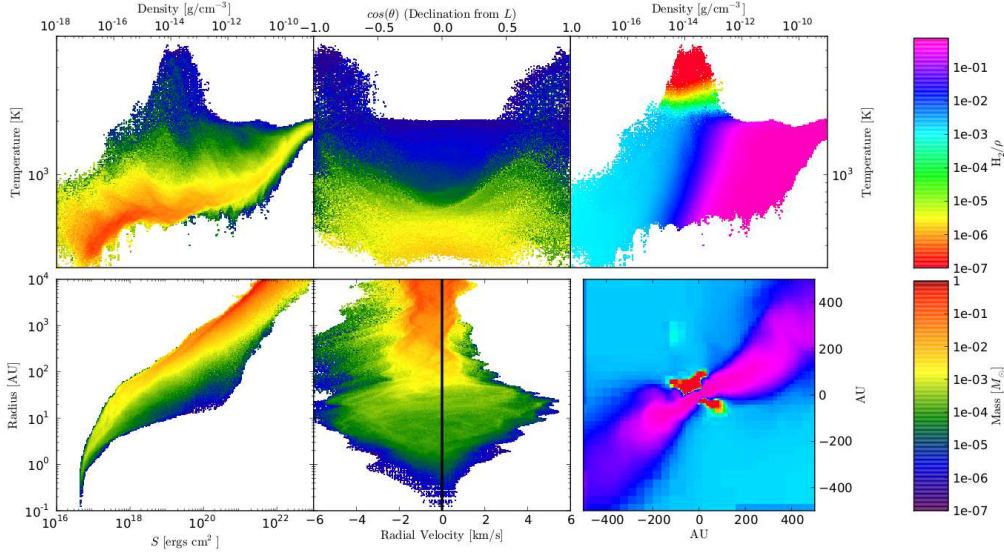


Fig. 1.— We show the distributions of the thermodynamic and kinetic states of the inner  $10^4$  AU of a collapsing primordial Population III star-forming region gas as a function of different variables: mass distribution as a function of density and temperature (upper left); mass distribution as a function of the declination (co-latitude) angle from the local angular momentum vector and temperature (upper middle); mass-weighted average molecular hydrogen mass fraction as a function of density and temperature (upper right); mass distribution as a function of radius from the center and an entropy-like quantity (lower left); mass distribution as a function of the radius and the local radial velocity of the gas (lower middle). In the lower right panel, we show a slice through the center of the simulation of the molecular hydrogen mass fraction. The field of view in the slice image is 1000 AU. Colorbars showing the molecular hydrogen fraction in each of the molecular hydrogen fraction plots and the mass in each pixel of the mass-distribution plots have been placed on the far right, in the upper and lower panels respectively.

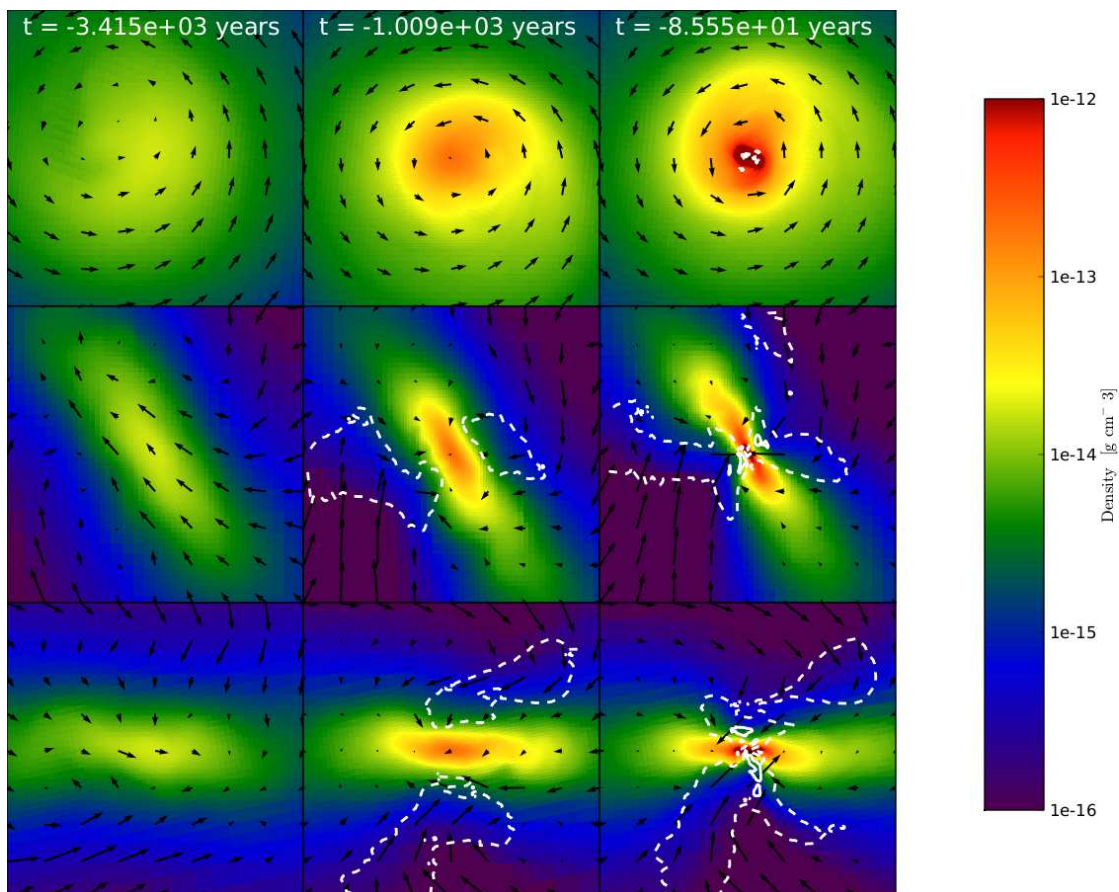


Fig. 2.— Slices at three different epochs (columns) in the collapse of the primordial cloud. The field of view in all images is 2000 AU on a side. The axes of alignment of the three rows have been chosen in an orthogonal frame (not the computational axes) where the normal vector of the top image is aligned with the angular momentum vector of the innermost 2000 AU of the disk, and the middle and lower rows are mutually orthogonal. Overplotted are velocity vectors and a contour at  $T = 1000$  K. From left, the times of the images are 3415, 1700, 1000, 320, and 85 years prior to the final output of the simulation.

phase space, similar to those shown in Abel et al. (2002); Yoshida et al. (2006); Turk et al. (2009); O’Shea & Norman (2007). However, we note the strong presence of low-mass regions of high-temperature gas, particularly at densities between  $10^{-15}$  g cm $^{-3}$  and  $10^{-13}$  g cm $^{-3}$ .

In the upper middle panel of Figure 1 we have plotted the distribution of mass in the innermost  $10^4$  AU of the halo as a function of the temperature and the cosine of declination from the average angular momentum vector at that radius. We have chosen cosine to ensure equal latitudinal area across the entire domain. In the normalization used here, the two extremes ( $-1.0$  and  $1.0$ ) correspond to the polar regions and the middle region ( $0.0$ ) corresponds to the disk region. All gas above a temperature of roughly 2000 K is confined within 60 degrees from the poles defined by the local angular momentum vector.

The upper right panel of Figure 1 shows the mass-weighted average molecular hydrogen mass fraction as a function of density and temperature. All of the gas above 2000 K is mostly or completely dissociated and free of molecules. The lower-temperature gas follows a typical transition from atomic to molecular states.

In the lower left panel of Figure 1 we have plotted the distribution of mass with respect to radius from the densest point of our cloud ( $x$ -axis) and an entropy-like quantity ( $S$ ,  $y$ -axis) defined by

$$S = \frac{k_b}{m_H} \frac{T}{\mu \rho^{2/3}},$$

where  $T$  is the temperature,  $\mu$  is the mean molecular weight and  $\rho$  is the density. Between 10 AU and 100 AU the high-temperature regions are visible as a broadening in the entropy profile, indicating a difference in the entropy gradient within the collapsing region.

In the lower middle panel of Figure 1 we plot the mass distribution as a function of distance from the densest zone and the radial velocity with respect to that zone. The velocity of the central zone in the calculation has been subtracted prior to calculation of the radial velocity. Several independent flow lines are visible, including several with net outward motion, particularly within  $\sim 50$  AU. The bulk flow is inward and the spread in velocities very close to the central point is expected as a result of both rotation and incoherent flow.

The lower right panel of Figure 1 gives a slice through the core, aligned with the  $y$ -axis, 1000 AU on a side, where the color corresponds to the molecular hydrogen mass fraction. We note the obvious molecular hydrogen-dominated disk and atomic high temperature polar regions.

In Figure 2, we display slices through the primordial cloud that are aligned with a new

orthogonal reference frame such that the normal to the image plane is aligned with the angular momentum vector of the innermost 2000 AU of the region. Overlaid are velocity vectors and contours at temperatures of 1000 K (dotted) and 2000 K (solid). Each column corresponds to a different epoch in the cloud’s collapse, where time of 0.0 years is the final output of the calculation. The upper panel shows disk settling at densities of approximately  $10^{-14}$  g cm $^{-3}$ . This disk undergoes little evolution over the displayed epochs in the top, face-on view, In the middle and lower panels, gas is flowing along the poles of the disk to the central point. High-temperature gas develops in these polar regions, at and above 2000 K, although we note that the largest pockets of hot gas are at 1000 K and extend nearly 1000 AU.

## 4. Discussion

### 4.1. Chemical Origin and Stability

The formation of molecular hydrogen at densities greater than  $10^{-16}$  g cm $^{-3}$  is dominated by the three-body formation mechanism, where two hydrogen atoms and a catalyst produce a single molecule of hydrogen. Formation through this channel produces an excited molecule of hydrogen, which rapidly collisionally de-excites to its ground state, depositing 4.48 eV of thermal energy in the gas. Conversely, collisional dissociation of a molecule of hydrogen removes from the gas 4.48 eV of thermal energy. As the formation and destruction rates of molecular hydrogen via these processes decrease and increase, respectively, with the temperature of the gas, this reduction in thermal energy carries with it a corresponding reduction in the rate at which molecular hydrogen associates. This process can be viewed as an increase in the specific heat of the gas; every molecule of hydrogen that is to be dissociated requires the introduction of 4.48 eV of energy. The equilibrium density of atomic hydrogen, at a fixed temperature and subject only to the three-body process and its inverse, can be written as:

$$n_{\text{H,eq}} = \frac{-1}{4k_{22}}(k_{13} - \sqrt{8k_{13}k_{22}n_{\text{H,H}_2} + k_{13}^2}). \quad (1)$$

where  $k_{13}$  is the dissociation rate in units of cm $^3$  s $^{-1}$  and  $k_{22}$  is the association rate in cm $^3$  s $^{-1}$ ,  $n_{\text{H,eq}}$  is the atomic hydrogen density in cm $^{-3}$  and  $n_{\text{H,H}_2}$  is the number density of the mixed hydrogen gas. In our simulation, we used values for  $k_{22}$  from Glover (2008) and  $k_{13}$  from Martin et al. (1996). As shown in the upper right panel of Figure 1, when gas exceeds roughly 2300 K at a density of  $10^{-14}$  g cm $^{-3}$ , the destruction rate dominates and the gas rapidly dissociates, but reaching or breaching that temperature barrier requires an influx of energy to dissociate any molecules of hydrogen. We note that while the temperature at which dissociation dominates will be weakly dependent on density, as seen in Equation 1. Having

less energy “locked up” in hydrogen molecules lowers the energy barrier to dissociation, as the gas can shed less energy via dissociative cooling.

In the absence of shocks, asymmetries or other perturbations of the gas, as in spherically-symmetric, 1D calculations, molecular hydrogen that is allowed to cool will simply slow its collapse if its temperature reaches the temperature at which the dissociative process dominates. The gas will loiter until radiative processes are able to shed enough thermal energy to allow it to collapse further. However, in our simulations, the gas may be subject to asymmetric inflow, minor shocks and disk formation, as discussed in Abel et al. (2002); Turk et al. (2009); Clark et al. (2010); Stacy et al. (2010); O’Shea & Norman (2007). Additionally, our physical model includes optical thickness to ro-vibrational cooling and our simulation resolves inhomogeneities of the density and temperature of the gas, both factors that change this evolution.

With a smaller specific heat as a result of a lower molecular fraction, the molecular hydrogen can be dissociated by minor shocks and other perturbations from infalling gas; once it has reached high temperatures, the energy barrier to associating molecular hydrogen is just as high, but with no mechanism for shedding thermal energy until compressional heating drives the temperature to  $\sim 10^4$  K. In the time-series plots in Figure 2 we show that the flow, while largely quiescent, features strong asymmetric inflow as well as fast infall along the poles. This produces a shocked, high-temperature gas which is subsequently compressionally heated.

At this point, the gas will be able to cool efficiently enough that it will likely not heat further, but it will also be unable to form substantial amounts of molecular hydrogen. This transition is shown in the upper right panel of Figure 1, where the high-temperature, shocked regions in the upper left panel are shown to have fully dissociated their reservoir of molecular hydrogen, and thus the only available coolant. We also draw attention to the power-law stratification in the molecular hydrogen fraction as a function of density and temperature, indicating an equilibrium molecular hydrogen fraction at those temperatures.

In the bottom left panel of Figure 1, we can identify two features in the entropy of the gas. The first is that the entropy overall decreases with decreasing radii; the cloud is globally stable against convection, which would require a reversal of the entropy gradient. However, the warm gas behaves adiabatically, retaining essentially constant entropy with decreasing radius. During subsequent accretion onto the protostellar cloud, this gas will continue to be confined by colder, radiatively efficient gas. Although globally stable against convection, at later times these adiabatic regions may undergo convective instability. In the final output plotted in Figure 2 (bottom rightmost image) we note that a pocket of gas of  $\sim 1000$  K has become distended and nearly disconnected from its innermost component; this may be the



start of a buoyant path, up and to the right in the image plane.

## 4.2. Radial Velocity and Disk Structure

In the lower middle panel of Figure 1, we can identify several distinct “tracks” along which gas is flowing. Each of the hot, dissociated regions is characterized by amplification of the inward radial velocity and a relatively small radial extent. Gas is falling inward onto the hot atomic bubbles, where it dissociates, increases in pressure, and then builds up on the inward side of the velocity spikes. This variance in the radial velocity of the shocked, dissociated regions results in gas that is collapsing less slowly; in the comoving frame of its surroundings, it may even be rising, although we cannot determine this at the stopping point in our simulation.

As seen in Figure 2, in this simulation a clear disk is formed, accentuated by the strong differences in the chemical and thermal states of the gas in the disk and in the polar regions. Examining the angular distribution of gas (Figure 1, upper middle panel) we see that the shocks are essentially confined to within or near the polar regions of the disk, demonstrated as well in the lower right panel of Figure 1. The mechanism by which Population III protostellar feedback will break out of the disk, as well as the density structure of a settled disk both require an understanding of this material, as the gas flowing along the poles will necessarily interact with these high-entropy regions. In past theoretical works discussing the accretion mechanism onto primordial protostars, radiative breakout has been identified as the sole mechanism by which accreting material flowing along the poles could be slowed or stopped (McKee & Tan 2008). This scenario may change if the polar regions are largely composed of high-temperature, atomic gas that is buoyant or unstable to convection. We propose that a chemical component may contribute to changes in the accretion flow even before the onset of radiative feedback from the central protostar, at times later than those probed in this simulation. The decreased molecular opacities in the polar region will allow protostellar accretion luminosity to reach larger radii, feeding back on the accretion flow.

## 5. Conclusions

The hydrodynamics of disk formation around a protostar lead to high temperature atomic polar regions. Until compressional heating drives the temperature of these hot, dissociated regions to  $10^4$  K, they have no opportunity for radiative cooling. The initial formation of these bubbles is through shocks dominated by large scale flows, and the chemical

processes that govern their evolution will continue to enable their formation. We see these dissociated regions prior to the formation of the central protostar, and we extrapolate that they will continue to persist until the protostar begins to accrete. Clearing material from the polar regions of the accretion disk, previously thought to be exclusively through radiative feedback mechanisms, is necessary to reverse accretion flows along the polar directions and enable the breakout of ionizing radiation. However, the process of terminating accretion along the polar regions of the accretion disk may be assisted by these hot regions, either by the dredging of material via buoyant or convective rising of material, or simply through the chemical and kinetic processes that prevent the region from associating molecular hydrogen. This may contribute to a much earlier breakout of radiation from the protostellar core than found in the models of McKee & Tan (2008), although (as noted in that paper) the total mass of gas flowing along the poles is much lower than that accreted from the disk.

The spread in the chemical, thermal and kinetic states of the gas as it regimes such as where we see these shocking regions, must be resolved to understand the mechanism by which accretion disks develop and matter is processed. One-dimensional codes, or codes that assume a universal equation of state as a function of density, are unable to do so. Furthermore, simulation codes that are unable to resolve the development and persistence of shocks, or that are otherwise unable to apply adequate resolution, are equally unable to resolve this formation and settling of a disk and its subsequent evolution. Future simulations that bypass the Courant condition, such as sink particles (as in Clark et al. (2010); Stacy et al. (2010)) while still resolving the relevant chemical and hydrodynamical processes, will be necessary to study the long term impact of these hot, atomic polar regions.

M.J.T. acknowledges support by NASA ATFP grant NNX08AH26G and NSF AST-0807312. These simulations were conducted utilizing the Triton Resource at San Diego Supercomputer Center. The authors thank Greg Bryan, Jeff Oishi, Britton Smith and Brian O’Shea for helpful comments, as well as Stephen Lepp, David Collins, Paul Clark, Simon Glover and Ralf Klessen for productive discussions. We thank the anonymous referee for thoughtful comments and suggestions.

## REFERENCES

- Abel, T., Anninos, P., Zhang, Y., & Norman, M. L. 1997, *New Astronomy*, 2, 181
- Abel, T., Bryan, G. L., & Norman, M. L. 2002, *Science*, 295, 93
- Bryan, G. L., Abel, T., & Norman, M. L. 2001, *ArXiv Astrophysics e-prints*

- Bryan, G. L. & Norman, M. L. 1998, *ApJ*, 495, 80
- Clark, P. C., Glover, S. C. O., Klessen, R. S., & Bromm, V. 2010, ArXiv e-prints
- Galli, D. & Palla, F. 1998, *A&A*, 335, 403
- Glover, S. 2008, in American Institute of Physics Conference Series, Vol. 990, First Stars III, ed. B. W. O’Shea, A. Heger, & T. Abel, 25–29
- Glover, S. C. O. & Abel, T. 2008, *MNRAS*, 388, 1627
- Jarosik, N., Bennett, C. L., Dunkley, J., Gold, B., Greason, M. R., Halpern, M., Hill, R. S., Hinshaw, G., Kogut, A., Komatsu, E., Larson, D., Limon, M., Meyer, S. S., Nolte, M. R., Odegard, N., Page, L., Smith, K. M., Spergel, D. N., Tucker, G. S., Weiland, J. L., Wollack, E., & Wright, E. L. 2010, ArXiv e-prints
- Martin, P. G., Schwarz, D. H., & Mandy, M. E. 1996, *ApJ*, 461, 265
- McKee, C. F. & Tan, J. C. 2008, *ApJ*, 681, 771
- Omukai, K. & Nishi, R. 1998, *ApJ*, 508, 141
- O’Shea, B. W., Bryan, G., Bordner, J., Norman, M. L., Abel, T., Harkness, R., & Kritsuk, A. 2004, ArXiv Astrophysics e-prints
- O’Shea, B. W. & Norman, M. L. 2007, *ApJ*, 654, 66
- Palla, F., Salpeter, E. E., & Stahler, S. W. 1983, *ApJ*, 271, 632
- Ripamonti, E. & Abel, T. 2004, *MNRAS*, 348, 1019
- Sobolev, V. V. 1960, *Moving envelopes of stars* (Cambridge: Harvard University Press, 1960)
- Stacy, A., Greif, T. H., & Bromm, V. 2010, *MNRAS*, 403, 45
- Turk, M. J., Abel, T., & Norman, M. L. 2010a, *ApJ*, in Preparation
- Turk, M. J., Abel, T., & O’Shea, B. 2009, *Science*, 325, 601
- Turk, M. J., Abel, T., & O’Shea, B. W. 2008, in American Institute of Physics Conference Series, Vol. 990, First Stars III, ed. B. W. O’Shea, A. Heger, & T. Abel, 16–20
- Turk, M. J., Clark, P. C., Glover, S. C. O., Greif, T. H., Abel, T., Klessen, R. S., & Bromm, V. 2010b, *ApJ*, submitted (June, 2010)

Verwer, J. G. 1994, *SIAM J. Sci. Comput*, 15, 1243

Yoshida, N., Omukai, K., Hernquist, L., & Abel, T. 2006, *ApJ*, 652, 6